Mathematical and Computational Applications, Vol. 11, No. 3, pp. 173-180, 2006.

COMPUTATIONAL MODELING OF FLOW INSIDE A DISEASED CAROTID BIFURCATION

Nurullah Arslan
Fatih University, Graduate Institute of Sciences and Engineering
& Department of Industrial Engineering
B. Çekmece, Istanbul, Turkey, 34500
narslan@fatih.edu.tr

Abstract- One of the leading causes for death after heart diseases and cancer in all over the world is still stroke. Most strokes happen because an artery that carries blood uphill from the heart to the head is clogged. Most of the time, as with heart attacks, the problem is atherosclerosis, hardening of the arteries, calcified buildup of fatty deposits on the vessel wall. The primary troublemaker is the carotid artery, one on each side of the neck, the main thoroughfare for blood to the brain. Only within the last twenty-five years, though, have researchers been able to put their finger on why the carotid is especially susceptible to atherosclerosis. In this study, the fluid dynamic simulations were done in a diseased carotid bifurcation under the steady flow conditions computationally. Reynolds numbers representing the steady flow were 300, 1020 and 1500 for diastolic, average and systolic peak flow represented by pulsatile flow waveform, respectively. In vivo geometry and boundary conditions were obtained from a patient who has stenosis located at external carotid artery (ECA) and internal carotid artery (ICA) of his common carotid artery (CCA). The location of critical flow fields such as low wall shear stress (WSS), stagnation regions and separation regions were detected near the highly stenosed region and at branching region.

Keywords: Carotid bifurcation, Stenosis, Arteriosclerosis, Wall Shear Stress.

1. INTRODUCTION

The formation of atherosclerosis has been reported due to the low or high shear regions. These regions develop at the downstream of the carotid bifurcation that is located in bifurcation part of the carotid arteries in humans. The low and high shear regions correlation with the atherosclerosis region were discussed by [1], [2] and stated the close correlation to the formation of lesions [2], [3], [4], and [5]. Arterial bifurcation studies have shown that the stress level in the bifurcating areas is several times higher than that in a straight segment. The effect of the arterial wall tension in the formation of atherosclerosis was proposed by [6], who suggested that atherosclerotic plaques occurred more frequently at wall locations where wall tension would be expected to be elevated. More researchers such as [7] and [8] reported that increased tensile stress predisposes tissue to atheroschelerosis. Nevertheless, most of theses studies have been confined to either the arterial wall itself ignoring the pulsatile flow of blood, or the blood flow domain alone assuming non-distensible walls. There only a few numerical studies that have treated both pulsatile flows and compliant walls, [9], [10], and [11].

2. MATERIALS AND METHODS

The *in vivo* geometry data and flow conditions were obtained from a male patient, who has two-sided atherosclerosis, at Cerrahpasa Medical School, Istanbul, Turkey, Figure 1. His age was 50 years old. He was smoker and normotensive. Imaging of the left carotid artery was done with color Doppler ultrasound. After imaging the flow in color Doppler scan mode, a static Doppler sample volume was deposited in the center of the carotid artery and the bifurcating vessels, spanning approximately one third of the vessel diameter. A marker was aligned with the vessel axis, and the angle between the Doppler line of sight and the vessel axis was computed. The velocity trace for the graft showed much higher velocities than in normal arteries, with a low pulsatility index since the sonograph trace remained well above zero throughout the cycle. For the patient shown in Figure 2, the instantaneous mean of the sonograph trace at the inlet was estimated to be 0.68 m/s average, maximum 1m/s and 0.2 m/s minimum.

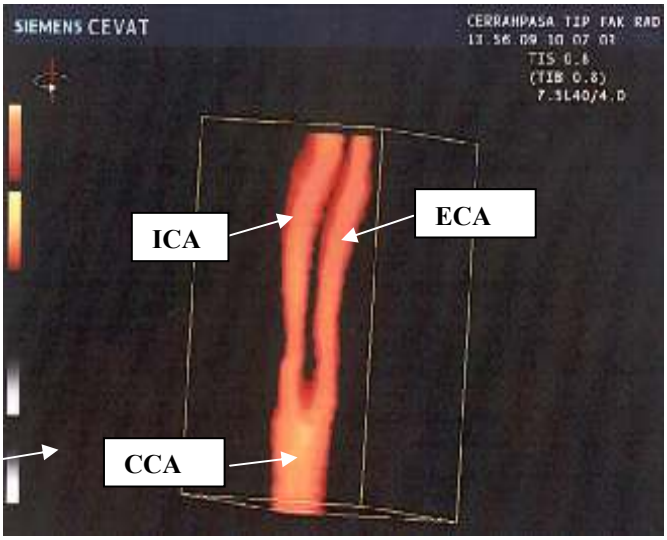

Figure 1. The geometry of the stenosed carotid artery taken by Color Doppler Ultrasound Imaging technique.

Measurements were also made in the arterial branch site. The velocity value was about 2 m/s at the most stenosed location and around 1.3 m/s at downstream of the stenosis, Figure 2, A-B-C.

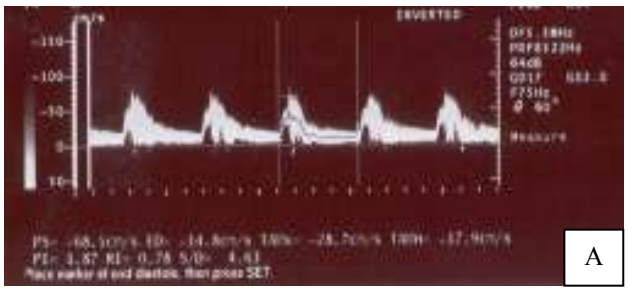

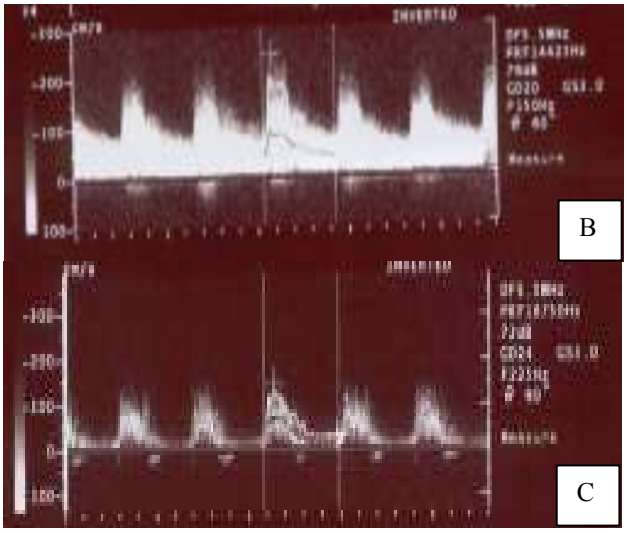

Figure 2. Velocity profiles inside the different regions of the carotid artery taken by color Doppler Ultrasound. A) Inlet B) Most Stenosed C) Downstream of the stenosis.

Spectral broadening was detected at the most stenosed location. Carotid model was created on the basis of images supplied by the cardiac surgeons representing the typical alternative designs, Figure 1. 3-D model of typical carotid arteries for a diseased patient was utilized using ACIS-based solid modeler Gambit (Fluent Inc., Lebanon, NH, USA) where the 3-D model and mesh were also created, Figure 4. The diameter of the entrance artery was taken as five millimeters in diameters from the color Doppler image. The model was meshed with an automatic meshing algorithm using tetrahedral elements. Reynolds number for the carotid inlet is difficult to estimate, since the shape of the velocity profile is unknown and the sample volume did not cover the whole vessel lumen. Based on the velocity measured in the sample volume (V), and assuming normal blood viscosity (μ = 3.5 mPa s), the above measurements lead to a systolic peak Reynolds number of 1500 and a diastolic minimum of 300 ($Re = \rho VD/\mu$, where ρ = blood density, 1050 kg/m^3). The entrance velocities were selected as 1 m/s at average, and 0.2 m/s at diastolic flow, respectively. Physiological forcing function used to drive the inlet velocity boundary condition as a function of time, Figure 3. The commercial finite volume code Fluent, Fluent Inc., Lebanon, NH, USA was used in this study. A segregated solver was selected and a convergence criterion was selected as 10^{-8}. The model was meshed with an automatic meshing algorithm using tetrahedral elements. Simulations were performed on a double Pentium (R) 4 CPU 2,8 GHz with 2,048 MB of RAM. Velocity profile at the inlet of the carotid artery was assumed flat. The true profile is something between flat and parabolic; if one assumes a relationship between spatially averaged and centerline velocity midway between these extremes, the Reynolds number is reduced by 25%. The true *in vivo* Reynolds number therefore remains unknown however, the range appears to span the laminar in a circular pipe ($Re_{critical} \approx 2300$).

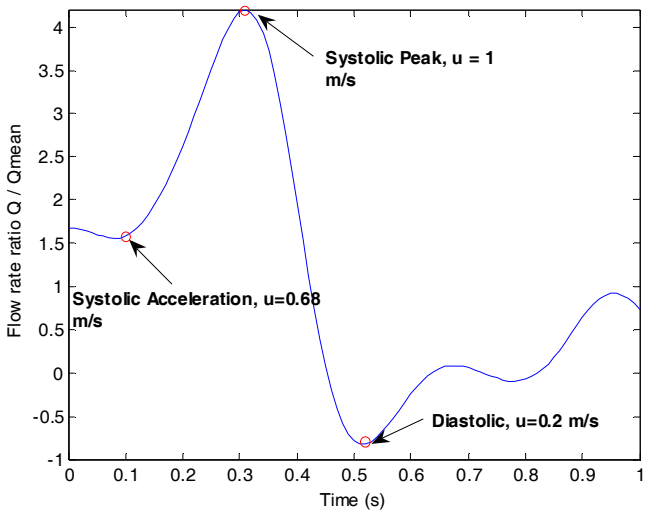

Figure 3. Physiological forcing function used to drive the inlet velocity boundary condition as a function of time.

2.1 Computational grid

All geometrical data were input into a specialized preprocessing program for grid generation. In total, 60,803 grid nodes were utilized giving rise to 286,848 computational tetrahedral. Figure 4 shows details of the utilized non-structured grid of the human carotid artery.

2.2 Flow equations, boundary flow conditions, and solution

The blood velocity was assumed uniform at the orifice of carotid. The applied inflow conditions mimic typical carotid blood flow velocity, 0.68 m/s, under resting condition. The values of the outflow discharges as percentages of the inlet flow are seventy-five percent from Internal carotid Artery

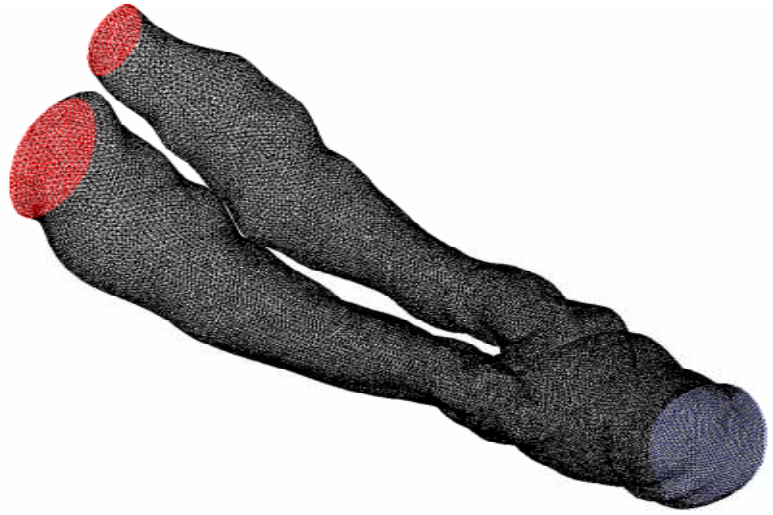

Figure 4. Mesh formation for diseased carotid artery

(ICA) to twenty-five percent from External Carotid Artery (ECA). All computational grid data, as well as all physical flow data determined from the boundary conditions, were imported into the main Computational Fluid Dynamics solver (FLUENT Inc.,) [12]. The numerical code solves the governing Navier–Stokes flow equations. In the generality, these equations solve the mass, momentum and energy conservation. The assumptions made about the nature of the flow are that it is three-dimensional, steady, laminar, isothermal, with no external forces applied on it while the arterial wall is comprised of non-elastic and impermeable material. In their generality time dependent governing equations for incompressible flow are

$$\frac{\partial \rho}{\partial t} + \frac{\partial \rho}{\partial x_i}(\rho u_i) = S_m \tag{1}$$

where ρ (kg/m^3) is the density, t (s) is the time, u_i (m/s) are the velocity components along the x_i, (m) axis, while S_m is the added or subtracted mass of fluid in the flow field. Equation 1 becomes for steady flow as

$$\frac{\partial \rho}{\partial x_i}(\rho u_i) = S_m \tag{2}$$

Unsteady conservation of momentum equation along the *i* direction is written as

$$\frac{\partial}{\partial t}(\rho u_i) + \frac{\partial \rho}{\partial x_j}(\rho u_i u_j) = -\frac{\partial p}{\partial x_i} + \frac{\partial \tau_{ij}}{\partial x_j} + \rho g_i + F_i \tag{3}$$

Here, ρ (N/m^2) is the static pressure, τ_{ij} (N/m^2) is the shear stress tensor, ρg_i (N/m^3) and F_i (N/m^3) are gravity and externally acting forces, respectively. For steady flow equation 3 becomes

$$\frac{\partial \rho}{\partial x_j}(\rho u_i u_j) = -\frac{\partial p}{\partial x_i} + \frac{\partial \tau_{ij}}{\partial x_j} + \rho g_i + F_i \tag{4}$$

The WSS, denoted by τ (N/m^2), is calculated as

$$\tau = \mu \dot{\gamma} \tag{5}$$

Where μ is the viscosity defined for incompressible fluid and the strain rate as

$$\dot{\gamma} = \frac{\partial u_i}{\partial x_j} + \frac{\partial u_j}{\partial x_i} \tag{6}$$

The components of the WSS possibly have different effects upon endothelial cells. Some components, mainly those being diagonal, generate intercellular tension, while the off-diagonal components possibly contribute to intercellular shearing forces.

3. RESULTS

The fluid flow characterization of the flow inside a diseased carotid bifurcation was analyzed computationally. Figure 5 shows the velocity vectors inside the diseased carotid artery together with the ICA and ECA. SI units were used. The flow enters the model with a flat velocity profile. The peak Reynolds number was 1500 at the inlet. The flow went through ICA and ECA and accelerated through the internal and external carotid arteries due to the reduction in cross-sectional area. The flow separation region at downstream of the branching point was seen by retrograde vectors. The artery stenosis on both left and right carotid arteries was seen in these specific patients. The velocities inside the stenosis region are increased similar to the jet flow. Depending on the internal geometry of the diseased artery, the circulation regions were seen not only at the inner surface of the branches but also on the external surface of the branches. The maximum velocity was found as 2.2 m/s at the narrowest region of the flow inside the internal carotid artery. The endothelial cells inside the arteries are very sensitive to the high and low shear stress regions. The regions found here would cause the increase of the intimal hyperplasia if there was no surgery done which will also cause the increase of the thickness of the diseased region more. This will cause the sudden ischemia for the patient who may result the patient to get killed or to get his brain affected. The plots clearly show the nature of secondary flow inside these regions. The shear stress distribution on the wall is illustrated in Figure 6. The highest WSS was seen at downstream of the carotid branching. The lower WSS region was found where the fluid circulation occurs on both sides of the branches. The structure of the internal part of the carotid was highly complex after stenosis formation.

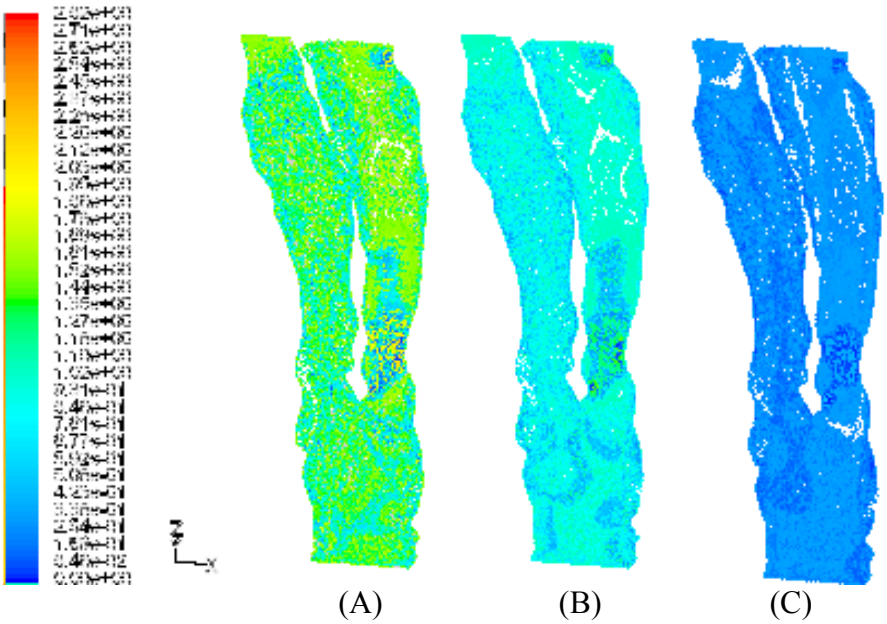

Figure 5: Velocity distribution (m/s) inside the diseased carotid artery along the bifurcation plane at various points of cardiac cycle, A) u=1 m/s, B) u=0.68 m/s, C) u=0.2 m/s

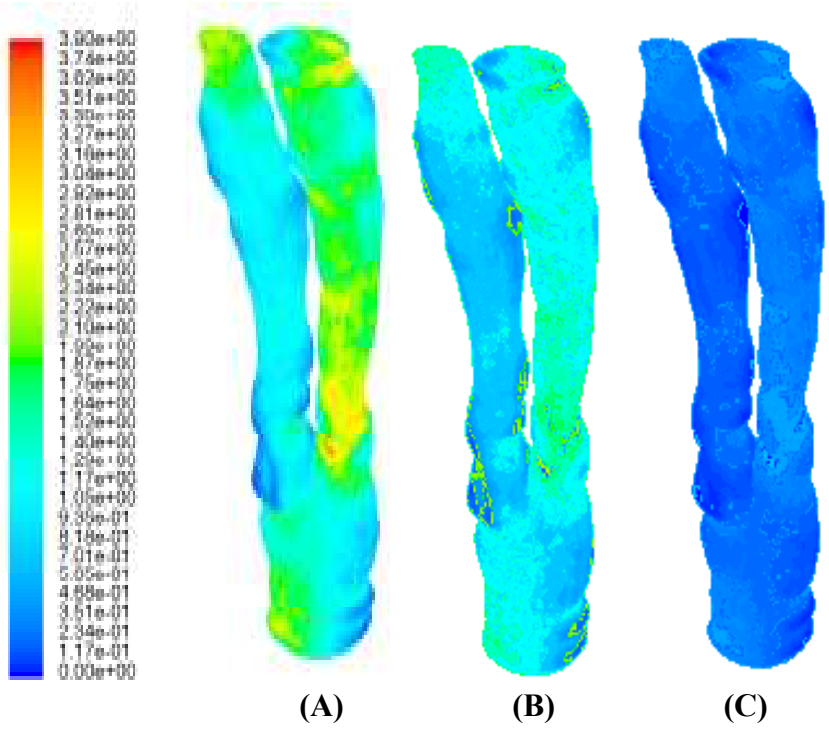

Figure 6. Wall shear stress distributions (in pascal) at the wall for diseased carotid artery at various points of the cardiac cycle, A) u = 1 m/s, B) u = 0.68 m/s, C) u = 0.2 m/s

4. CONCLUSIONS

Computational analysis of the flow field inside diseased carotid arteries for a male patient was performed The flow was found similar to the flow inside a branching channel. The geometry of the stenosis inside the diseased carotid artery defines the flow characterization. When the inner diameter gets smaller, the flow rate will increase which will cause the high shear stress regions. The geometry due to the atheroschelerosis formation inside the internal and external branching caused the flow circulated and low WSS. The upscaled experimental model of the diseased artery will be better to study to understand the flow regions with a higher spatial resolution in future. In addition, the effect of the critical flow regions on the endothelial cells in vivo will be considered for the future studies to understand the mechanics of the real formation of the atherosclerosis.

Acknowledgement
I would like to thank to Surgeon Kazim Beşirli from the department of cardiovascular surgery of Cerrahpaşa Medical School, University of Istanbul for sharing the color Doppler images and his recommendations regarding the reading of the images with me. I also would like to thank to Professor Hikmet Kocabaş from Mechanical Engineering department of Istanbul Technical University for his valuable discussion regarding the numerical studies.

5. REFERENCES

1. D.L. Fry, Acute vascular endothelial changes associated with increased blood velocity gradients, *Circ Res.* 22(2), 165–197, 1968

2. C.G. Caro, J.M. Fitz-Gerald, R.C. Schroter, Atheroma and arterial wall shear. Observation, correlation and proposal of a shear dependent mass transfer mechanism for atherogenesis, *Proc R Soc Lond B Biol Sci.,* 177(46), 109–159, 1971

3. D.N. Ku, D.P. Giddens, C.K. Zarins, S. Glagov, Pulsatile flow and atherosclerosis in the human carotid bifurcation. Positive correlation between plaque location and low oscillating shear stress, *Arteriosclerosis*, 3, 293–302, 1985

4. S.G. Friedman, B.A. Kerner, M.S. Friedman, C.G. Moccio, Limb salvage in elderly patients. Is aggressive surgical therapy warranted?, *J Cardiovasc Surg* (Torino), 30(5), 848–851, 1989

5. I. Korner, R. Blatz, I. Wittig, D. Pfeiffer, C. Ruhlmann, Serological evidence of Chlamydia pneumoniae lipopolysaccharide antibodies in atherosclerosis of various vascular regions, *Vasa.,* 28(4), 259–263, 1999

6. S. Glagov, D.A. Rowley R.I. Kohut, Atherosclerosis of human aorta and its coronary and renal arteries. A consideration of some hemodynamic factors which may be related to the marked differences in atherosclerotic involvement of the coronary and renal arteries, *Arch Pathol.* 72, 558–571, 1961

7. M.E. DeBakey, G.M. Lawrie, D.H. Glaeser, Patterns of atherosclerosis and their surgical significance, *Ann Surg.,* 201(2), 115–131, 1985

8. M.J. Thubrikar, F. Robicsek, Pressure-induced arterial wall stress and atherosclerosis, *Ann Thorac Surg.,* 59(6), 1594–1603, 1995

9. Z. Lou, W.J. Yang, A computer simulation of the blood flow at the aortic bifurcation with flexible walls, *J Biomech Eng.* 115(3), 306–315, 1993

10. K. Perktold, G. Rappitsch, Computer simulation of local blood flow and vessel mechanics in a compliant carotid artery bifurcation model, *J Biomech.,* 28(7), 845–856, 1995

11. J.R. Cebral, R. Lohner, P.L. Choyke, P.J. Yim, Merging of intersecting triangulations for finite element modeling, *J Biomech.* 34(6), 815–819, 2001

12. K.M. Kelkar and S.V. Patankar, Development Of Generalized Block Correction Procedures For The Solution Of Discretized Navier-Stokes Equations, Computer Physics Communications, 53 (1-3), 329-336, 1989